3D Finite Element Computation of Laser Cavity Eigenmodes

Konrad Altmann

LAS-CAD GmbH, Brunhildenstr. 9, 80639 München, Germany,
Dr.Altmann@las-cad.com

Christoph Pflaum

Universität Erlangen, Lehrstuhl für Informatik X, Cauerstr. 6, 91058 Erlangen, Germany, pflaum@informatik.uni-erlangen.de

David Seider

Universität Würzburg, Institut für Angewandte Mathematik und Statistik, Am Hubland, 97074 Würzburg, Germany, seider@mathematik.uni-wuerzburg.de

A new method for computing eigenmodes of a laser resonator by the use of finite element analysis (FEA) is presented. For this purpose, the scalar wave equation $[\Delta + k^2]\,\tilde{E}(x, y, z) = 0$ is transformed into a solvable 3D eigenvalue problem by separating out the propagation factor $\exp(-ikz)$ from the phasor amplitude $\tilde{E}(x, y, z)$ of the time-harmonic electrical field. For standing wave resonators, the beam inside the cavity is represented by a two-wave ansatz.

For cavities with parabolic optical elements the new approach has successfully been verified by the use of the gaussian mode algorithm. For a DPSSL with a thermally lensing crystal inside the cavity the expected deviation between gaussian approximation and numerical solution could be demonstrated clearly.

OCIS codes: 140.3410, 140.4780, 000.4430, 140.3580, 140.6810.

1. Introduction

Since the laser was invented, its development has been supported continuously by theoretical models, which have been able to describe the physics of the laser to a high degree. But there are still open problems, and modern laser technology demands powerful numerical tools, for instance to model thermal lensing and gain guiding effects in laser cavities, or to predict the efficiency of laser configurations. Those tools generally involve the computation of the transverse eigenmodes of a laser cavity, meaning solutions of Maxwell's equations for a propagating beam with certain boundary conditions being imposed.

Since in lasers the transverse variations of the refractive index are usually small, Maxwell's equations can be replaced by the scalar wave equation

$$\left[\Delta + k^2\right] \tilde{E}(x, y, z) = 0 \tag{1}$$

where $\tilde{E}(x, y, z)$ is the phasor amplitude of a field distribution that is sinusoidal in time. $k = 2\pi/\lambda$ is the propagation constant of the optical wave in the medium, where λ is the wave length in the medium. The most common way to solve this equation for a propagating beam is through the paraxial wave equation (see for instance Ref. 1, Chapt. 16).

In the special but significant case that the beam is propagating through spherical (or more specifically, parabolic) dielectric interfaces, gaussian ducts, i.e. parabolic distributions of refractive index and gain, or is reflected on spherical mirrors, analytical solutions of the paraxial wave equation are available in the form of the well known Hermite-gaussian polynomials. In real situations, the gaussian mode algorithm can successfully be applied, if the distributions of refractive index and gain in laser crystals can be approximated by parabolic fits. This approach for instance is used in the laser cavity code LASCAD$^{\text{TM}}$.[2,3]

There are, however, situations where the gaussian mode algorithm is not sufficient, and therefore a full numerical analysis is needed. For this purpose, since the early work of Fox and Li,[4] instead of the partial differential equation (PDE) (1) an equivalent integral equation is traditionally involved, based on the so-called round-trip condition (see Ref. 1, Chapt. 14, for example). This means that a propagation integral acts on a wavefront $\tilde{E}(x_0, y_0)$ at a certain reference plane to produce a new optical field describing the wavefront at the same reference plane but after one round trip through the cavity. To represent an eigenmode, the recirculated wavefront must meet the eigenvalue equation

$$\gamma_{nm}\tilde{E}_{nm}(x, y) = \iint \tilde{K}(x, y, x_0, y_0)\tilde{E}_{nm}(x_0, y_0)\ \mathrm{d}x_0\ \mathrm{d}y_0 \tag{2}$$

where the kernel $\tilde{K}$ of the propagation operator depends on the properties of the cavity, and γ_{nm} is a complex eigenvalue. Equation (2) lends itself to try a solution by an iterative application of the integral operator, an approach that has been used in many modifications since the pioneering work of Fox and Li.

In modern computer codes, a beam propagation method (BPM) is used to compute a series of round-trips starting with a more or less arbitrary initial field distribution. The iteratively recirculated field distribution finally converges to the lowest-order mode or to a superposition of higher order transversal modes, dependent on the losses of the latter ones. However, convergence of this procedure cannot be predicted in general. Even if the procedure converges to the lowest-order mode, usually an admixture of higher order modes remains, making it difficult to isolate the exact shape of the lowest-order mode. Essentially, two methods have been proposed to extract particular eigenmodes by sampling the fluctuating distributions of the optical field, generated by the repeated iterations, at a certain reference plane along the propagation axis.

In 1981, Feit and Fleck[5] published an approach that uses the computation of a field correlation function whose Fourier transform with respect to the propagation axis reveals the eigenvalues as resonant peaks. The eigenvalues obtained in this way are used to generate the mode eigenfunctions by carrying through additional discrete Fourier transforms of the field. The accuracy of the obtained eigenvalues increases inversely proportional to the number of iterations, and therefore, in real situations a

high number of iterations is required. A more serious drawback consists in the fact that the geometrical length of the cavity being analyzed is restricted. This problem has not been specially pointed out by Feit and Fleck, but it follows from Equation 16 in their work, which states that the maximum bandwidth $\Delta\beta$ of the spectrum obtained for the propagation constant is restricted by $\Delta\beta = \pi/\Delta z$, where Δz is the path length of one round trip. Physically, this means that the field fluctuations due to the superposition of modes with different propagation constants must be slow enough to be resolved by the sampled field patterns. Since in laser resonators $\Delta\beta$ as well as Δz cannot be chosen arbitrarily, this approach fails for longer resonators with internal elements, as can be shown if one applies the method to long resonators that can also be analyzed by the use of the gaussian mode algorithm.

An alternative method also using repeatedly sampled field distributions, known as the Prony method, has been introduced by Siegman and Miller[6] in 1970. This method is designed to determine the coefficients and arguments for a time function

$$f(t) = \sum_{j=1}^{N} K_j \exp(p_j t) \tag{3}$$

composed of N complex exponential functions from a sequence of $2N$ complex values $f(nt), n = 1, 2, \ldots, 2N$, which are generated by forming the scalar products of $2N$ subsequently generated field patterns. N is the number of dominant eigenmodes assumed to be present in the pattern used to start the iterations. The Prony method primarily addresses the problem of eigenvalue determination. The computation of eigenmodes must be carried through in a subsequent step. In the literature available to us, we could not find information on how exact eigenvalues and eigenmodes can be computed by the use of this method.

Both methods referenced above use field patterns generated in a first step to compute eigenvalues in a second, and eigenmodes in a third step. Therefore, they depend on the numerical accuracy of these primarily generated patterns. Practical experience with BPM shows that fluctuations due to limited computational accuracy can affect the appearance of these patterns. Therefore, it seems advantageous to develop a method that primarily addresses the computation of eigenmodes, since they are needed mainly to analyze the properties of a laser cavity.

Another approach to calculating eigenmodes of an optical cavity is to discretize the scalar wave equation or the original Maxwell's equations directly by applying the finite element method. This was done, for instance, by Streiff, Witzig, and Fichtner[7] for simulating VCSEL devices. The main difficulty of this approach is that for geometries large compared with the wavelength, a huge number of discretization grid points is necessary to resolve the oscillations of the propagating wave. Furthermore, the system of linear equations obtained by a finite element discretization can be very ill-conditioned in the case of the scalar wave equation, which additionally increases the computational time enormously. Therefore, Streiff, Witzig, and Fichtner applied a 2D reduction by symmetry assumptions. In many practical situations, however, such symmetry assumptions are not appropriate.

In this paper we present a new approach to compute the eigenmodes and eigenvalues of optical resonators. Our approach also uses finite element analysis (FEA), but

different from Streiff, Witzig, and Fichtner, we separate out small scale oscillations of the field $\tilde{E}$ by the use of a factorization that allows for increasing the mesh size in z-direction by orders of magnitude and therefore drastically reduces the number of nodes needed to obtain sufficient accuracy. Furthermore, compared with methods that use an integral operator as referenced above, which only involve iteratively computed field distributions at a single reference plane, our method is based immediately on the differential equation (1) and therefore solves the eigenvalue problem simultaneously on the whole resonator domain.

2. Derivation of a Solvable Eigenvalue Problem for the Laser Modes

A laser cavity is a device where an electro-magnetic wave propagates in a periodically guiding structure. 'Guiding structure' means, that distributions of a complex valued refractive index, and optical elements like lenses and mirrors, are grouped along a main axis of propagation in a way that only a small part of the propagating electro-magnetic energy is leaking out the sides of the cavity to infinity. 'Periodically' means, that a substructure of finite length $\tilde{L}$ along the propagation direction exists, and that the full periodic structure is obtained by an identical reproduction of the substructure after $z = n\tilde{L}, (n = 1, 2, ...)$, where the propagation direction is assumed to coincide with the z-axis. Therefore, we write

$$\tilde{E}(x, y, z) = \exp\left[-ik_f z + i\psi(z)\right] \tilde{v}(x, y, z). \tag{4}$$

The term $\psi(z)$ takes into account that a guided wave generally has a propagation constant, which is smaller than the propagation constant k_f of the free wave, as well known from texts on wave guide or laser theory (see Siegman,[1] Chapt. 19.3). If the guiding structure is independent of z, that means if $\tilde{L} \to 0$ as in common wave guides, $\psi(z)$ can be replaced by εz, where ε is a small real quantity. In laser cavities, this generally is not the case. For instance, in simple two mirror resonators, $\psi(z)$ for the lowest-order gaussian mode is given by the Guoy phase shift (see for instance Ref. 1, Chapt. 19.3)

$$\psi(z) = \arctan \frac{z}{z_R}, \tag{5}$$

where z_R is the Rayleigh range. Equation (5) shows that, in this case, the maximum variation of $\psi(z)$ along the resonator axis from the left to the right mirror is confined to $-\pi \leq \psi(z) \leq \pi$. For higher-order gaussian modes $\psi(z)$ is restricted by integer multiples of π, depending on the mode order. In the case of general paraxial resonators, which may be composed of mirrors and lenses, and weakly guiding refractive index distributions of finite length, it therefore seems reasonable to use εz instead of $\psi(z)$ and to take into account the remaining phase fluctuations $\varepsilon z - \psi(z)$ in a function $\tilde{u} = \exp\left[-i(\varepsilon z - \psi(z))\right] \tilde{v}$, which delivers

$$\tilde{E}(x, y, z) = \exp\left[-i(k_f - \varepsilon)z\right] \tilde{u}(x, y, z). \tag{6}$$

Equation (5) shows, that the phase fluctuations $\varepsilon z - \psi(z)$ can be assumed small along propagation distances of the order of the wave length. Therefore, $\tilde{u}$ overall

can be expected to be free of small scale spatial oscillations with a scale length corresponding to the wavelength. This leads to the important conclusion, that an efficient FEA discretization with a mesh size of the order of the wave length or even much larger should be possible.

To take into account small fluctuations of the refractive index, we define

$$k = k_f + k_s(x, y, z), \tag{7}$$

where k_s generally is a complex valued quantity of small modulus. Then, insertion of equations (6) and (7) into (1) delivers

$$-\Delta\tilde{u} + 2i(k_f - \varepsilon)\frac{\partial\tilde{u}}{\partial z} - k_s(2k_f + k_s)\tilde{u} = \varepsilon(2k_f - \varepsilon)\tilde{u}. \tag{8}$$

Since in most interesting cases $\varepsilon/k_f <\approx 10^{-4}$, the term ε in the first parenthesis on the left side and in the parenthesis on the right side usually can be neglected, delivering

$$-\Delta\tilde{u} + 2ik_f\frac{\partial\tilde{u}}{\partial z} - k_s(2k_f + k_s)\tilde{u} = 2\varepsilon k_f\tilde{u} =: \xi\tilde{u} \tag{9}$$

or

$$-\Delta\tilde{u} + 2ik_f\frac{\partial\tilde{u}}{\partial z} + (k_f^2 - k^2)\tilde{u} = \xi\tilde{u}. \tag{10}$$

If the beam guiding structure does not change along the propagation axis z, i.e. if k_s is independent of z, and therefore $\partial\tilde{u}/\partial z$ vanishes for stationary eigenmodes, Eq. (9) transforms into

$$\Delta_{x,y}\tilde{u} + 2k_f(\varepsilon + k_s)\tilde{u} = 0, \tag{11}$$

where additionally k_s^2 has been neglected. Equation (11) is identical with the 2D eigenvalue equation for weakly guiding structures, as well known from texts on wave guide theory.

Since we are looking for 3D eigenmodes, the solutions $\tilde{E}$ and its derivatives with respect to z must meet conditions of periodicity imposed by the length $\tilde{L}$ of the substructure. But since we are considering cavities with $\tilde{L} \gg \lambda$, the $\tilde{L}$-periodicity of the phase factor in Eq. (6) can always be achieved by a very small change of k_f that has negligible influence on Eq. (10). Therefore, we neglect this phase factor, and impose the conditions of periodicity directly on $\tilde{u}$ as follows

$$\begin{aligned} \tilde{u}(x, y, \tilde{L}) &= \tilde{u}(x, y, 0) \\ \frac{\partial}{\partial z}\tilde{u}(x, y, \tilde{L}) &= \frac{\partial}{\partial z}\tilde{u}(x, y, 0). \end{aligned} \tag{12}$$

Perpendicular to the propagation direction the laser modes usually strongly decay with distance from the axis, but since we are forced to use a finite computational volume, a non-reflecting boundary condition must be used for the transverse evanescent part of the wave. An appropriate choice is to use a Robin boundary condition

$$\frac{\partial\tilde{u}}{\partial\vec{n}} - iC_b\tilde{u} = 0, \tag{13}$$

where $\partial/\partial\vec{n}$ denotes the derivation in direction of the outer normal, and C_b can be chosen as $C_b = k_f$, see e.g. Ref. 8 and the references cited therein.

Equations (10), (12), and (13) describe a solvable eigenvalue problem for the cavity modes. To derive these equations, the only approximations were made when Eq. (8) was replaced by Eq. (10) and when a Robin boundary condition was used instead of a non-reflecting boundary condition.

For the FEA we define a domain as depicted in Fig. 1, where the mirrors shall be located at the left and right faces. We denote the cuboid of size $W \times W \times L$ by Ω, and the boundaries by Γ_0, Γ_1, and Γ_r, which stand for the left mirror, the right mirror, and the remaining open part of the boundary, respectively.

To compute the eigenmodes of a standing wave resonator, two waves, propagating in opposite directions and appropriately coupled at the mirrors, must be taken into account. For this purpose, we extend the above model by the use of the following two-wave ansatz:

$$\tilde{E}(x,y,z) = \exp\left[-i(k_f-\varepsilon)z\right]\tilde{u}_r(x,y,z) + \exp\left[-i(k_f-\varepsilon)(L-z)\right]\tilde{u}_l(x,y,z). \quad (14)$$

The functions $\tilde{u}_r$ and $\tilde{u}_l$ must meet the following boundary conditions at the end mirrors

$$\tilde{u}_r(x,y,0) = \underbrace{\exp\left[ik_f\left(\frac{x^2}{R_{1x}}+\frac{y^2}{R_{1y}}\right)-i\pi\right]}_{\phi_0(x,y):=}\tilde{u}_l(x,y,0), \quad (15)$$

$$\tilde{u}_l(x,y,L) = \underbrace{\exp\left[ik_f\left(\frac{x^2}{R_{2x}}+\frac{y^2}{R_{2y}}\right)-i\pi\right]}_{\phi_1(x,y):=}\tilde{u}_r(x,y,L),$$

where a phase shift of π, due to reflection, and an additional phase shift due to the curvature of the mirrors, has been taken into account. $R_{1x(y)}$ and $R_{2x(y)}$ are the radii of curvature in x- and y-direction of the left and the right mirror, respectively.

Combining all considerations above leads to a rigorous mathematical definition of a PDE eigenvalue problem for the computation of eigensolutions $(\tilde{u}_r, \tilde{u}_l)$ and complex eigenvalues ξ, as follows:

$$\begin{aligned} -\triangle\tilde{u}_r + 2ik_f\frac{\partial\tilde{u}_r}{\partial z} + (k_f^2-k^2)\tilde{u}_r &= \xi\tilde{u}_r \quad \text{and} \\ -\triangle\tilde{u}_l - 2ik_f\frac{\partial\tilde{u}_l}{\partial z} + (k_f^2-k^2)\tilde{u}_l &= \xi\tilde{u}_l \quad \text{in } \Omega \end{aligned} \quad (16)$$

with boundary conditions

$$\begin{aligned} \tilde{u}_r - \phi_0\tilde{u}_l &= 0 \quad \text{on } \Gamma_0, \\ \tilde{u}_r - \bar{\phi}_1\tilde{u}_l &= 0 \quad \text{on } \Gamma_1, \\ \frac{\partial\tilde{u}_r}{\partial z} + \phi_0\frac{\partial\tilde{u}_l}{\partial z} &= 0 \quad \text{on } \Gamma_0, \\ \frac{\partial\tilde{u}_r}{\partial z} + \bar{\phi}_1\frac{\partial\tilde{u}_l}{\partial z} &= 0 \quad \text{on } \Gamma_1, \end{aligned} \quad (17)$$

$$\begin{aligned}\frac{\partial \tilde{u}_r}{\partial \vec{n}} - iC_b\tilde{u}_r &= 0 \quad \text{on } \Gamma_r,\\ \frac{\partial \tilde{u}_l}{\partial \vec{n}} - iC_b\tilde{u}_l &= 0 \quad \text{on } \Gamma_r.\end{aligned}$$

3. Finite Element Discretization

To discretize the eigenvalue problem (16), (17), we apply the finite element method. A straight-forward application, however, would lead to an unstable discretization of the large first order terms $+2ik_f\frac{\partial \tilde{u}_r}{\partial z}$ and $-2ik_f\frac{\partial \tilde{u}_l}{\partial z}$ in equations (16). In the finite difference context, this can be circumvented by an upwind and downwind discretization of the first order terms, respectively. We prefer a stable finite element discretization based on the streamline diffusion method, since this delivers a more accurate discretization than the finite difference upwind and downwind discretization.[9,10] To obtain a suitable streamline diffusion discretization of the eigenvalue problem (16), (17), we add terms of order $O(h)$, which essentially represent an artificial viscosity in z-direction, to these equations.

Let $V_{h_{xy},h}$ be the space of complex valued tri-linear finite elements of a grid on Ω with mesh sizes h in z-direction and h_{xy} for the transversal directions. Furthermore, let

$$\mathcal{V} := \left\{(v_r, v_l) \in V_{h_{xy},h} \times V_{h_{xy},h} \,\middle|\, v_r - \phi_0 v_l|_{z=0} = 0 \text{ and } v_r - \bar{\phi}_1 v_l|_{z=L} = 0\right\} \tag{18}$$

be the product space of waves v_r and v_l, which travel in opposite directions and satisfy the coupling boundary conditions at the mirrors. Then, the stabilized variational formulation of (16), (17) reads:

Find $(u_r, u_l) \in \mathcal{V}$ and $\xi \in \mathbf{C}$ such that

$$\begin{aligned}&\int_\Omega \left(\nabla u_r \nabla \bar{v}_r + (k_f^2 - k^2)u_r\bar{v}_r + 2ik_f\frac{\partial}{\partial z}u_r\bar{v}_r\right)\,\mathrm{d}(x,y,z) - iC_b\int_{\Gamma_r} u_r\bar{v}_r\,\mathrm{d}\sigma(x,y,z)\\ &\quad + \tau h\int_\Omega \left(2ik_f\frac{\partial}{\partial z}u_r + (k_f^2 - k^2)u_r\right)\frac{\partial}{\partial z}\bar{v}_r\,\mathrm{d}(x,y,z)\\ &+ \int_\Omega \left(\nabla u_l \nabla \bar{v}_l + (k_f^2 - k^2)u_l\bar{v}_l - 2ik_f\frac{\partial}{\partial z}u_l\bar{v}_l\right)\,\mathrm{d}(x,y,z) - iC_b\int_{\Gamma_r} u_l\bar{v}_l\,\mathrm{d}\sigma(x,y,z)\\ &\quad - \tau h\int_\Omega \left(-2ik_f\frac{\partial}{\partial z}u_l + (k_f^2 - k^2)u_l\right)\frac{\partial}{\partial z}\bar{v}_l\,\mathrm{d}(x,y,z)\\ &\qquad = \xi\int_\Omega \left(u_r\overline{v}_r + \tau h\, u_r\frac{\partial}{\partial z}\bar{v}_r + u_l\overline{v}_l - \tau h\, u_l\frac{\partial}{\partial z}\bar{v}_l\right)\,\mathrm{d}(x,y,z)\end{aligned} \tag{19}$$

holds for all $(v_r, v_l) \in \mathcal{V}$, with appropriately chosen stabilization parameter $\tau \geq 0$.

This leads to a discrete eigenvalue problem

$$A(U_{r,h}, U_{l,h}) = \xi_h M(U_{r,h}, U_{l,h}), \tag{20}$$

where A on the left-hand side is the stiffness matrix and M on the right-hand side is the mass matrix of (19). $(U_{r,h}, U_{l,h})$ are the discrete eigenvectors with eigenvalue

ξ_h. By finite element theory, the convergence of this finite element approximation for $(h_{xy}, h) \to 0$ is guaranteed.

Our numerical experiments suggest, that the second derivatives $\partial^2/\partial z^2$ in Eqs. (16) only have negligible effect on the shape of the solution. However, different from BPM methods these terms do not complicate the computations in our approach, because they only enter when the stiffness matrix A is computed at the beginning of the algorithm.

4. Numerical Results

The eigenvalue problem (20) was solved by a shift-and-invert method. To solve the equations in the "invert-part" we used preconditioned GMRES.[11]

In this section, some results are presented which have been obtained using our new FEA approach. We have selected some configurations that allow for verification of our results by the use of the gaussian mode algorithm, since this is the only method permitting an exact analytical analysis of laser cavities. To show that our method is not confined to those cases, we also apply it to a cavity configuration that includes thermal effects and that cannot be computed satisfactorily with the gaussian ABCD algorithm.

Example 1. Our first example concerns a cavity consisting of a real gaussian duct (see e.g. Ref. 1, Chapt. 20) between planar end mirrors, i.e. a distribution of refractive index, showing a parabolic profile perpendicular to the propagation direction z, but being independent of z. In detail, we used the following dimensions:

- Distance between end mirrors $L = 0.1$ mm,
- wavelength $\lambda = 2.0$ μm,
- refractive index $n(x, y, z) = 1 - (n_2 \times r^2)/2$.

Using the two-wave ansatz, we performed the FEA computations on a domain with width $W = 0.2$ mm and with $40 \times 40 \times 5$ elements ($\approx$ 10000 grid points). For comparison, Table 1 shows the spot sizes w_{FEA} computed for three different values of n_2 by the use of our FEA method and w_{G} computed by the gaussian mode algorithm, respectively.

Since the refractive index is independent of z, the phase shift $\psi(z)$ in Eq. (4) can be replaced by εz. As for instance explained in Ref. 1, Chapt. 16.6, for the lowest-order gaussian mode ε_{G} is given by $\varepsilon_{\mathrm{G}} = (n_2)^{1/2}$. Table 1 shows the good correspondence of ε_{G} with $\varepsilon_{\mathrm{FEA}}$ deduced from the computed eigenvalue $\xi_h (= 2\,\varepsilon_{\mathrm{FEA}}\,k_f)$.

Example 2. Here we apply our method to an empty cavity of length $L = 1.0$ mm, whose left end mirror is concave with a radius of curvature $R_1 = 5.0$ mm, whereas the right mirror is planar. Figure 2 shows the spot size, as a function of z, of the lowest-order mode as obtained by our FEA code in comparison with the result of the gaussian algorithm. The width of the computational domain was $W = 0.2$ mm; in the computation $41 \times 41 \times 61$ ($\approx$ 102000) nodes have been involved.

Our derivation of the eigenvalue problem in Section 2 proves that the Guoy phase shift $\psi(z)$ can be computed by the use of the relation

$$\tilde{u}(0,0,z) = \exp\left[-i(\varepsilon z - \psi(z))\right] |\tilde{u}(0,0,z)|,$$

where $\tilde{u}$ and ε are the numerically obtained results for the eigenmode and the eigenvalue, respectively. Since $\psi(z)$ only is determined except for a constant, we set $\psi(L) = 0$ for this example. In Figure 3 the numerically computed phase shift $\psi_{\mathrm{FEA}}(z)$ and the gaussian phase shift $\psi(z)$ as given by Eq. (5) are plotted. The excellent agreement between both results shows that our method is able to predict even fine details exactly.

Example 3. To demonstrate that our method can reliably take into account focusing effects in longer cavities, we analyze in this example a cavity with planar end mirrors having a distance of $L = 10.0$ mm. Only a short section extending from the left mirror over 1.0 mm length is filled with a Gaussian duct, that means the refractive index is defined by $n(x, y, z) = 1 - (n_2(z) \times r^2)/2$ with

$$n_2(z) = \begin{cases} 0.06 & \text{if } z \leq 1.0 \\ 0.0 & \text{else.} \end{cases}$$

Figure 4 shows the z-dependence obtained for the spot size of the lowest-order mode by the use of FEA and by the gaussian code LASCAD$^{\mathrm{TM}}$,[2,3] respectively. Both results nearly coincide. The FEA has been carried through on a domain with width $W = 0.4$ mm. The grid was made up by $20 \times 20 \times 150$ elements, which corresponds to approximately 70000 points.

Figures 5 and 6 display the normalized intensity of the lowest-order and of one higher-order mode, respectively.

Example 4. In this example we use our method to model a monolithic DPSSL consisting of an end pumped Nd:YAG crystal, whose deformed end faces represent the end mirrors of the cavity. To take into account thermal lensing due to the temperature dependence of the refractive index and due to thermal distortion a thermal and structural FEA has been carried through by the use of LASCAD$^{\mathrm{TM}}$.[2] The data obtained in this way for the temperature distribution and deformation of the crystal have been imported into our program. We used a rectangular slab of equal height and width $W = 0.8$ mm and length $L = 8.0$ mm cooled from top and bottom, but not from left and right. The obtained temperature distribution therefore deviates strongly from rotational symmetry. Figure 7 shows the thermally induced refractive index distribution on the whole slab and Figure 8 along x- and y-axis immediately behind the entrance plane of the pump beam (at $z = 0$) as obtained with LASCAD$^{\mathrm{TM}}$.[2] To compute the mode shape by the use of a gaussian approximation as implemented in LASCAD$^{\mathrm{TM}}$,[2] the refractive index distribution is fitted parabolically for a series of cross sections along the z-axis as also shown in Figure 8 for a cross section close to $z = 0$. The obtained parabolic coefficients are used in a round trip ABCD matrix to compute the mode shape. Figures 9 and 10 show the spot sizes along the z-axis obtained in this way in comparison with the spot sizes obtained by our new approach that uses the full 3D thermal and structural FEA data without parabolic fit. For our

computations we used $80 \times 80 \times 32$ elements which equates to approximately 250000 grid points. As one can see, the results are very close to each other in the y-z-plane, whereas in x-z-plane the spot size obtained by our new approach is considerably larger. This is expected from the fact that the parabolic fit shown in Fig. 8 is good along the y-axis, but very poor along the x-axis for which the plot shows a bell shaped distribution. Accordingly, for the transverse mode profile the deviation between the gaussian profile and the result of the 3D approach also is much stronger along the x-axis than along the y-axis as shown in Figures 11 and 12.

5. Conclusions and Outlook

As referenced in the introduction, several methods for the numerical computation of the eigenmodes of laser cavities have been developed and still are widely used. Most of them are based on the early work of Fox and Li, using a round-trip integral operator to compute the field distribution at a reference plane iteratively. The sampled field distributions are used to compute eigenvalues and modes in subsequent steps. Since it seems impossible to guarantee applicability and accuracy of this integral method in general, we have presented a new approach, which addresses a direct solution of the partial differential equation (1) by methods of finite element analysis. Compared with the integral method, which can use data only at a single reference plane, the FEA approach allows for simultaneously involving the whole resonator domain into the numerical procedure.

Different from other approaches, which also apply FEA directly to Helmholtz or Maxwell's equations, we use a factorization to separate out the oscillating factor $\exp(-ikz)$ from the phasor amplitude $\tilde{E}(x, y, z)$ to obtain a function $\tilde{u}(x, y, z)$, whose variation with respect to z is relatively slow. This leads to a solvable eigenvalue problem for $\tilde{u}(x, y, z)$ as shown in Section 2. The factorization allows considerable reduction of the number of nodes necessary for sufficient resolution.

For cases that allow for application of the gaussian mode algorithm, our results are in excellent agreement with the latter one, as shown for several examples presented in Section 4. Curved end mirrors have been modeled by imposing appropriate boundary conditions, taking into account a locally varying phase shift.

Based on thermal and structural FEA results imported from LASCAD$^{\text{TM}}$,[2] we have also applied our method to model a monolithic DPSSL consisting of an end pumped crystal, whose deformed end faces represent the end mirrors of the cavity. In this case, the expected deviation between gaussian approximation and numerical solution could be demonstrated clearly. Therefore, the combination of our new approach with thermal and structural FEA is expected to deliver an accurate and reliable eigenmode analysis also for more complex resonator configurations.

Acknowledgment

We would like to thank the Bavarian Research Foundation for the financial support of this work.

References

1. A. E. Siegman, *Lasers* (University Science Books, Mill Valley, 1986).
2. LASCAD™, `http://www.las-cad.com`.
3. K. Altmann, "Simulation software tackles design of laser resonators," Laser Focus World **36(5),** 293–294 (2000).
4. A. G. Fox and T. Li, "Resonant modes in a maser interferometer," Bell Sys. Tech. J. **40,** 453–458 (1961).
5. M. D. Feit and J. A. Fleck, Jr., "Spectral approach to optical resonator theory," Appl. Opt. **20(16),** 2843–2851 (1981).
6. A. E. Siegman and H. Y. Miller, "Unstable optical resonator loss calculation using the Prony method," Appl. Opt. **9(10),** 2729–2736 (1970).
7. M. Streiff, A. Witzig, and W. Fichtner, "Computing optical modes for VCSEL device simulation," IEE Proc. Optoelectron. **149,** 166–173 (2002).
8. F. Ihlenburg, *Finite Element Analysis of Acoustic Scattering* (Springer, New York, Berlin, Heidelberg, 1998).
9. H.-G. Roos, M. Stynes, and L. Tobiska, *Numerical Methods for Singularly Perturbed Differential Equations* (Springer, Berlin, Heidelberg, 1996).
10. K. W. Morton, *Numerical Solution of Convection-Diffusion Problems.* (Chapman & Hall, London, New York, 1996).
11. Y. Saad and M. H. Schultz, "GMRES: A generalized minimal residual algorithm for solving nonsymmetric linear systems," SIAM J. Sci. Stat. Comput. **7,** 865–881 (1986).

Table 1. Comparison between FEA and Gaussian Results for a Gaussian Duct with Real Refractive Index

n_2	w_{FEA} [μm]	w_{G} [μm]	$\varepsilon_{\mathrm{FEA}}$	$\varepsilon_{\mathrm{G}} = \sqrt{n_2}$
0.24	36.220	36.049	0.497	0.490
0.48	30.376	30.313	0.708	0.693
0.72	27.714	27.391	0.871	0.849

List of Figure Captions

Fig. 1. Computational Domain. seiderFig1.eps.
Fig. 2. Empty cavity with one concave ($R_1 = 5.0$ mm) and one planar end mirror, FEA (solid line) and gaussian mode shape (dashed line). seiderFig2.eps.
Fig. 3. Guoy phase shift for an empty cavity with one concave ($R_1 = 5.0$ mm) and one planar end mirror, FEA (solid line) and gaussian mode shift (dashed line). seiderFig3.eps.
Fig. 4. Comparison between FEA (solid line) and gaussian results (dashed line) for a long resonator with a short gaussian duct attached to the left mirror. seiderFig4.eps. Double columned!
Fig. 5. Lowest-order mode in a long resonator. seiderFig5.eps. Double columned!
Fig. 6. TEM_{22}-mode in a long resonator. seiderFig6.eps. Double columned!
Fig. 7. Slice and isosurfaces of a refractive index distribution based on numerical data imported from LASCAD^{TM}. seiderFig7.eps. Double columned!
Fig. 8. Comparison of numerical (dots) and parabolically fitted (triangles) refractive index. Screen shot of LASCAD^{TM}. seiderFig8.eps.
Fig. 9. Comparison of FEA (solid line) and gaussian x-axis spot size (dashed line) along cavity axis for a monolithic laser with thermal effects taken into account. seiderFig9.eps. Double columned!
Fig. 10. Comparison of FEA (solid line) and gaussian y-axis spot size (dashed line) along cavity axis for a monolithic laser with thermal effects taken into account. seiderFig10.eps. Double columned!
Fig. 11. Transverse mode profile along x-axis for a monolithic laser with thermal effects taken into account, FEA (solid line) and gaussian mode result (dashed line). seiderFig11.eps.
Fig. 12. Coinciding transverse mode profiles along y-axis for a monolithic laser with thermal effects taken into account, FEA (solid line) and gaussian mode result (dashed line). seiderFig12.eps.

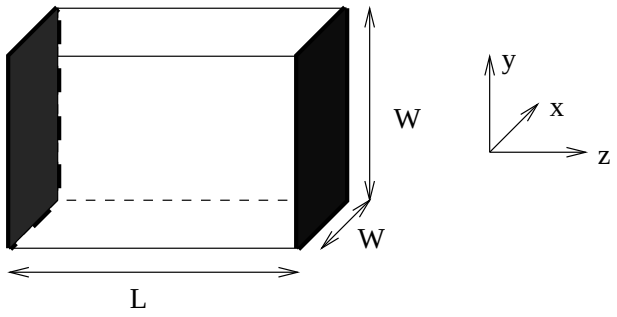

Fig. 1. Computational Domain. seiderFig1.eps.

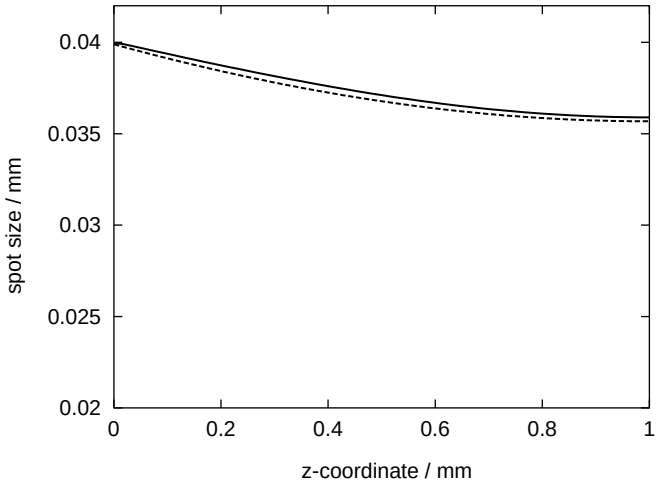

Fig. 2. Empty cavity with one concave ($R_1 = 5.0$ mm) and one planar end mirror, FEA (solid line) and gaussian mode shape (dashed line). seiderFig2.eps.

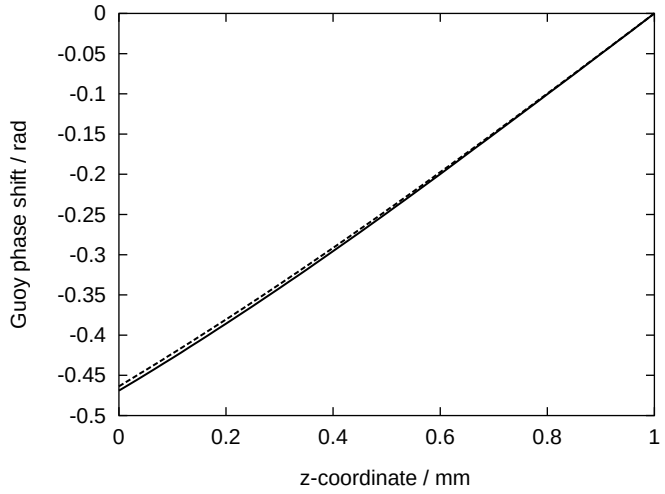

Fig. 3. Guoy phase shift for an empty cavity with one concave ($R_1 = 5.0$ mm) and one planar end mirror, FEA (solid line) and gaussian mode result (dashed line). seiderFig3.eps.

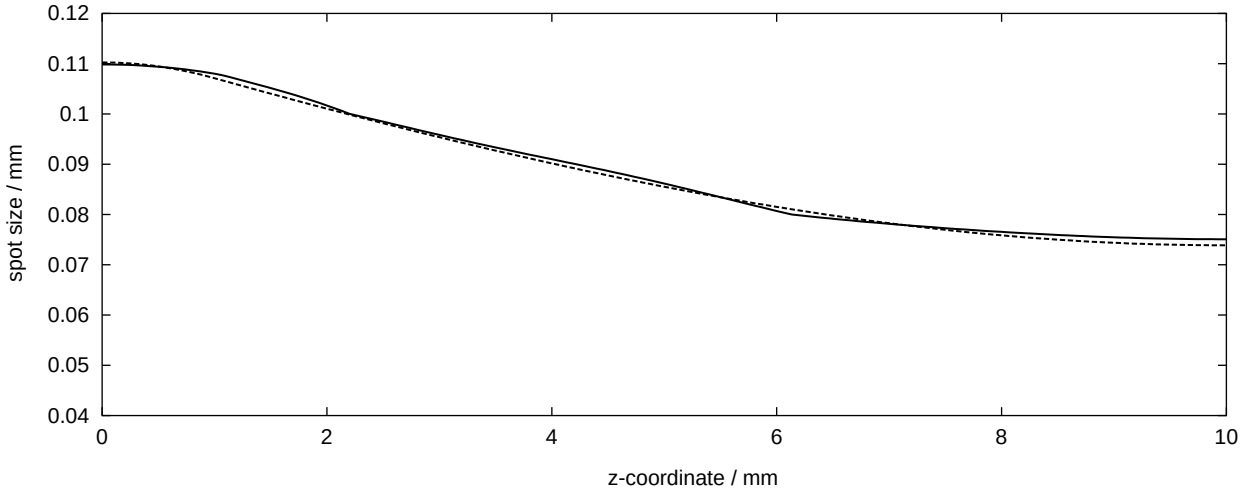

Fig. 4. Comparison between FEA (solid line) and gaussian results (dashed line) for a long resonator with a short gaussian duct attached to the left mirror. seiderFig4.eps. Double columned!

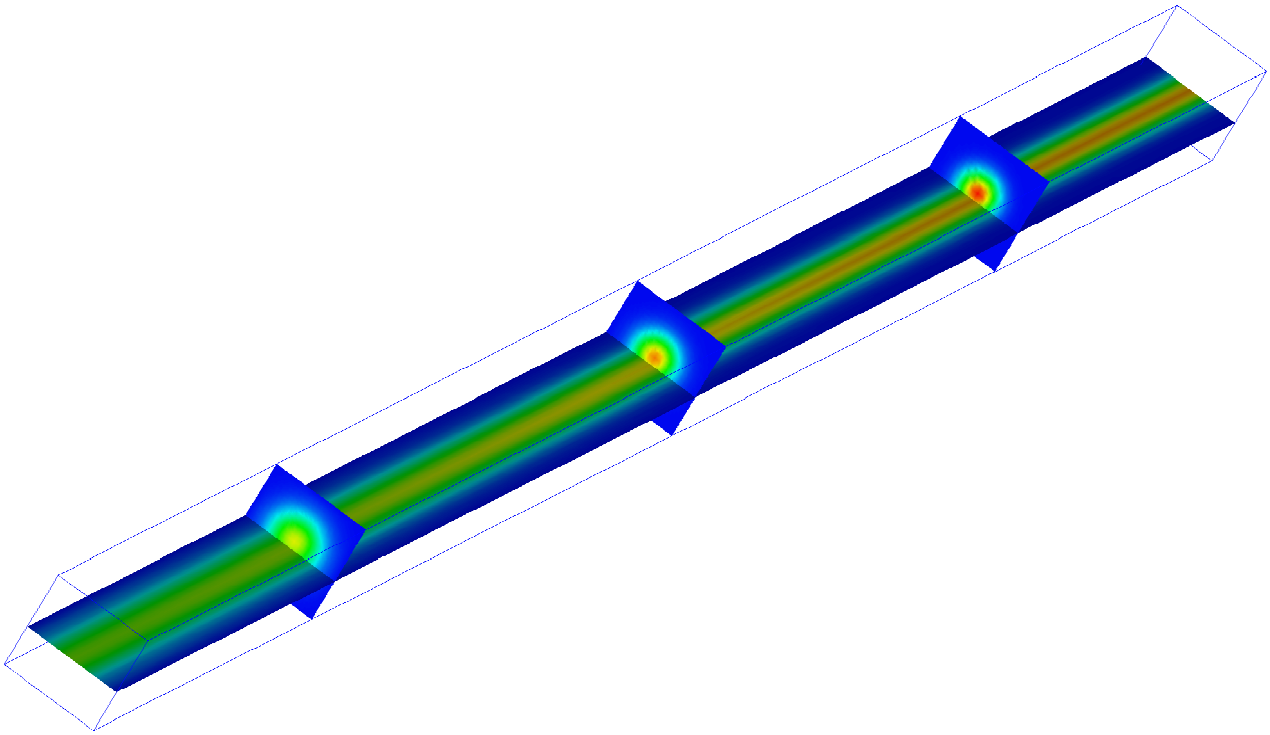

Fig. 5. Lowest-order mode in a long resonator. seiderFig5.eps. Double columned!

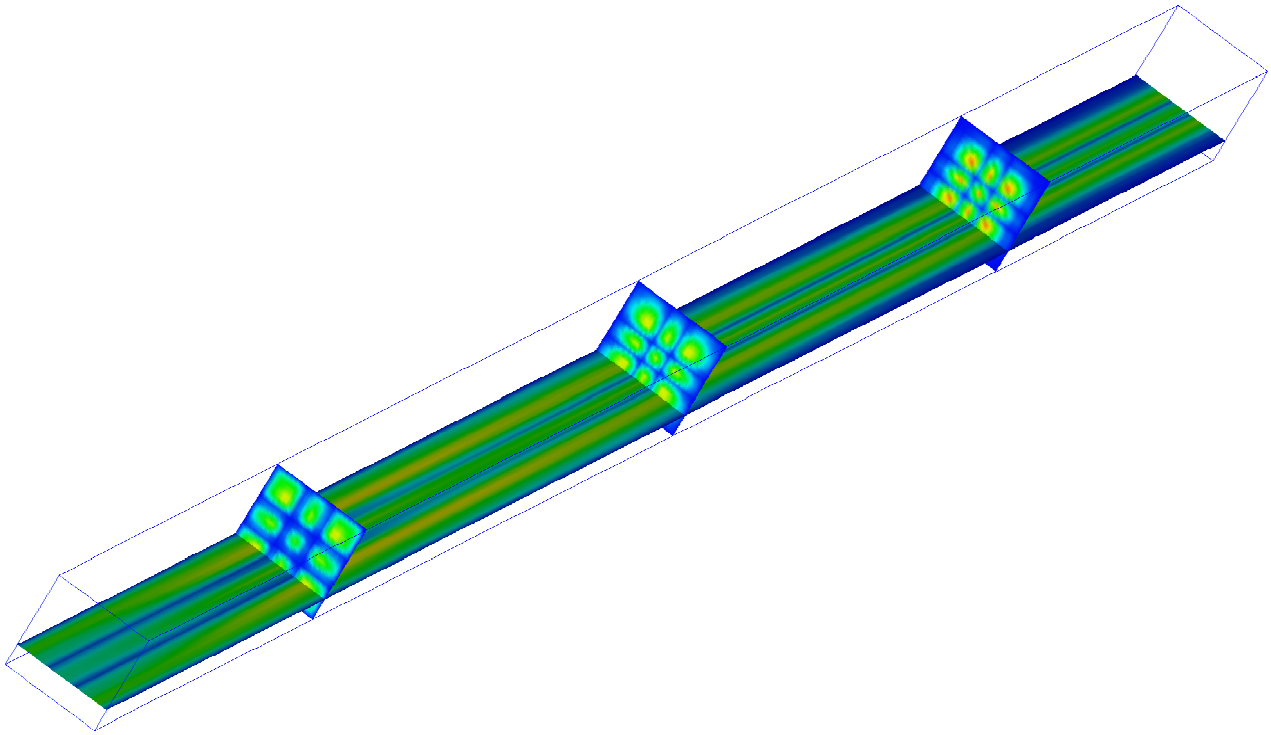

Fig. 6. TEM_{22}-mode in a long resonator. seiderFig6.eps. Double columned!

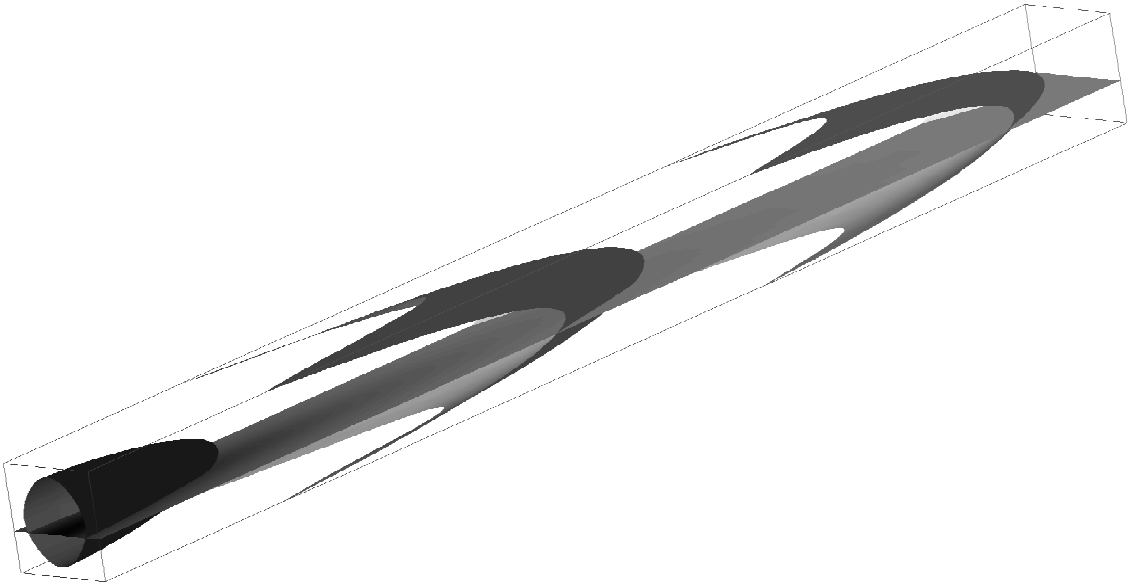

Fig. 7. Slice and isosurfaces of a refractive index distribution based on numerical data imported from LASCAD™. seiderFig7.eps. Double columned!

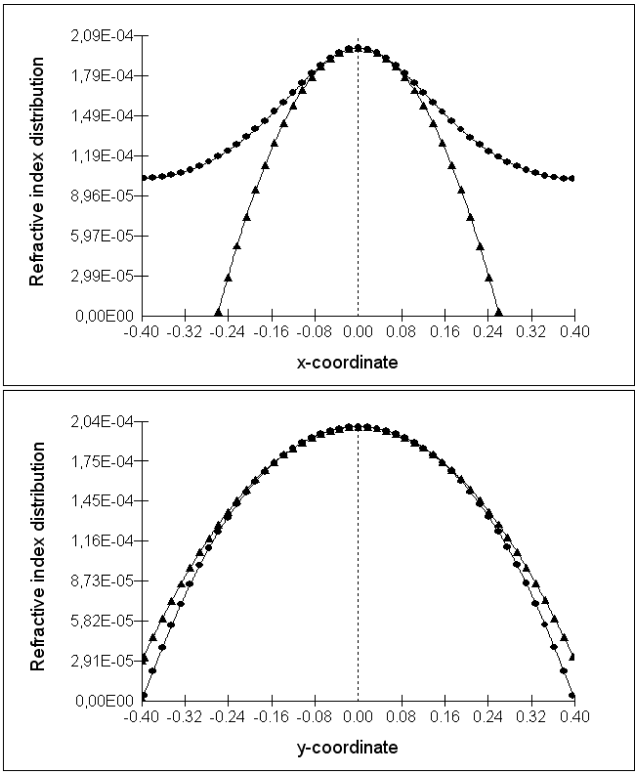

Fig. 8. Comparison of numerical (dots) and parabolically fitted (triangles) refractive index. Screen shot of LASCAD^{TM}. seiderFig8.eps.

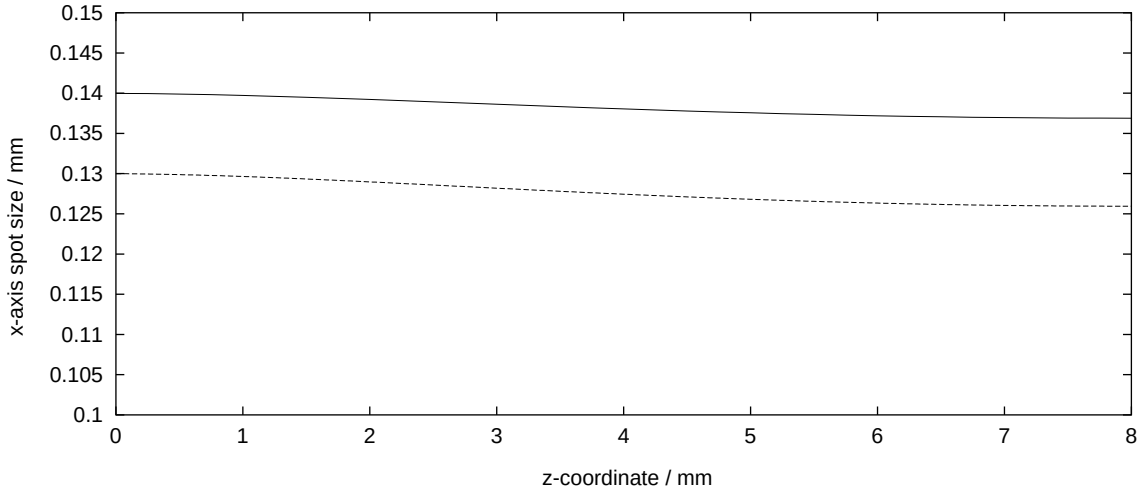

Fig. 9. Comparison of FEA (solid line) and gaussian x-axis spot size (dashed line) along cavity axis for a monolithic laser with thermal effects taken into account. seiderFig9.eps. Double columned!

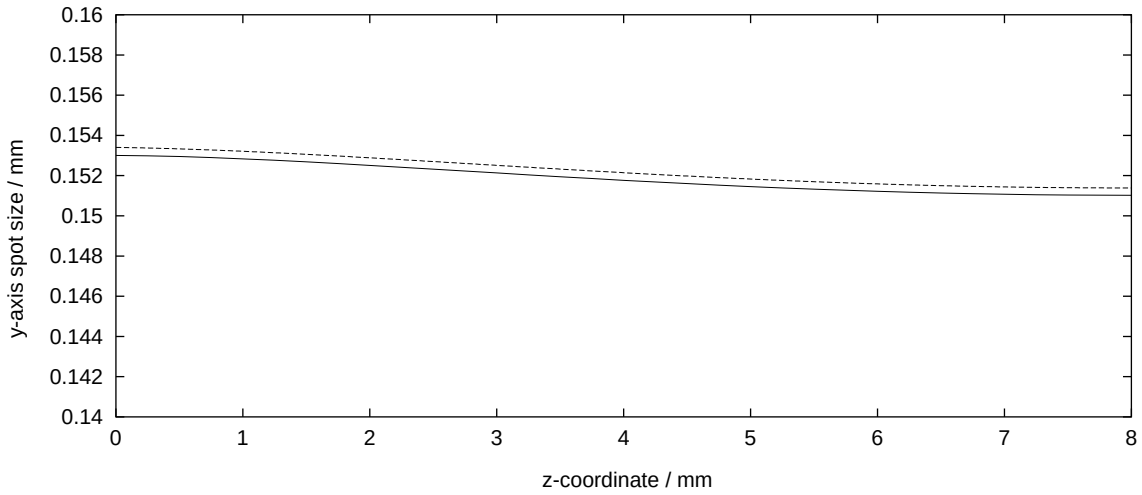

Fig. 10. Comparison of FEA (solid line) and gaussian y-axis spot size (dashed line) along cavity axis for a monolithic laser with thermal effects taken into account. seiderFig10.eps. Double columned!

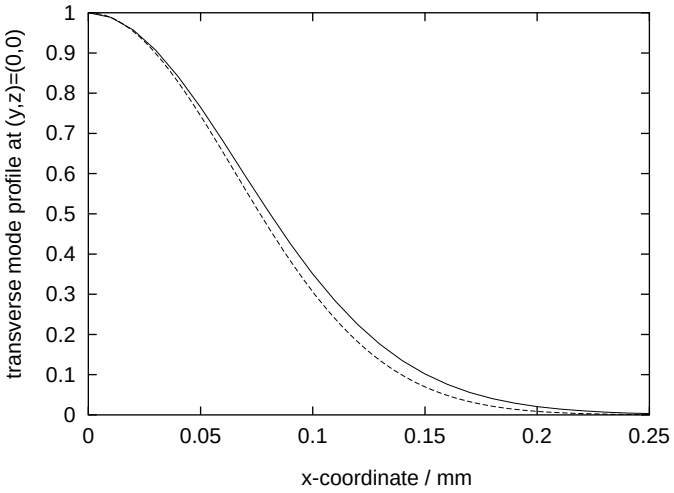

Fig. 11. Transverse mode profile along x-axis for a monolithic laser with thermal effects taken into account, FEA (solid line) and gaussian mode result (dashed line). seiderFig11.eps.

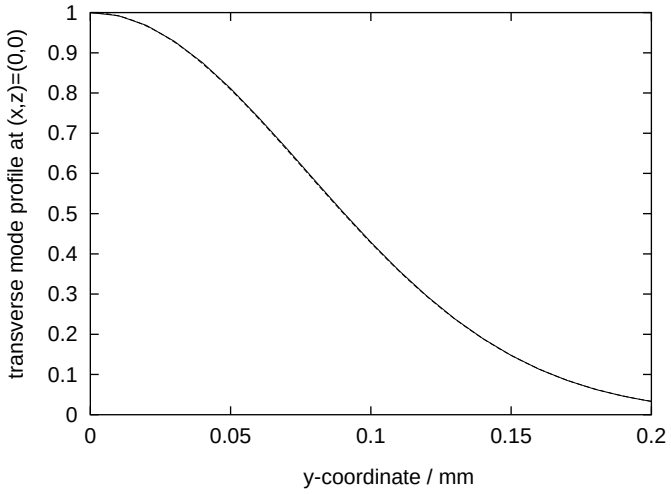

Fig. 12. Coinciding transverse mode profiles along y-axis for a monolithic laser with thermal effects taken into account, FEA (solid line) and gaussian mode result (dashed line). seiderFig12.eps.